PAF: A software tool to estimate free-geometry extended bodies of anomalous pressure from surface deformation data.

A.G. Camacho [1], J. Fernández [1,*], F. Cannavó [2]

[1] Institute of Geosciences (CSIC-UCM), Madrid, Spain

[2] Osservatorio Etneo, Istituto Nazionale di Geofisica e Vulcanologia, Catania, Italy.

_____

*Corresponding author:

Institute of Geosciences (CSIC-UCM), Fac. C. Matemáticas, Plaza de Ciencias, 3. 28040-Madrid.

Spain. e-mail: jft@mat.ucm.es; phone: +34-913944632

Abstract: We present a software package, namely PAF (acronym from authors' names), to carry out inversions of surface deformation data (any combination of InSAR, GPS, and terrestrial data) as produced by 3D free-geometry extended bodies with anomalous pressure changes. The anomalous structures are described as an aggregation of elementary cells (whose effects are estimated as coming from point sources) in an elastic half space. The linear inverse problem (considering some simple regularization conditions) is solved by means of an exploratory approach. This software represents the open implementation of a previously published methodology (Camacho et al., 2011). It can be freely used with large data sets (e.g. InSAR data sets) or with data coming from small control networks (e.g. GPS monitoring data), mainly in volcanic areas, to estimate the expected pressure bodies representing magmatic intrusions. Here, PAF software is applied to some real test cases.

Keywords: software, surface deformation, pressure sources, volcano monitoring.

1. Introduction.

In a volcanic context, surface deformation is related to the dynamics of volcanic plumbing systems, such as the shape of magma intrusions, magma pressure, and emplacement mechanisms (Masterlark, 2007). Surface deformation data are normally inverted to infer information about the intrusive pressure sources (e.g. Rymer and Williams-Jones, 2000; Dzurisin, 2003; Masterlark, 2007; Pedersen and Sigmundsson, 2006; Saltogianni et al., 2014). Normally, analytical solutions for regular geometries (point sources, disks, prolate or oblate spheroids, opening cracks, etc.) are employed at the initial stages to describe the surface deformation (Lisowski, 2007, Battaglia et al., 2013). Moreover, the mathematical model must consider some elastic properties to account for the response of the shallow crust to the pressure source. Usual analytical modeling assumes an elastic, homogeneous and isotropic crust, but it can take into account effects from several source geometries, topography relief and gravity (Williams and Wadge, 1998; Charco et al., 2007; Battaglia and Hill, 2009).

Camacho et al. (2011) presented an original methodology for the simultaneous inversion of vertical (Up), East-West (EW), and North-South (NS) deformation components and/or LOS InSAR displacement, by means of a 3D pressure distribution without any assumption on the source geometry. Assuming homogenous elastic conditions, the approach determines a general geometrical configuration of pressurized sources. The sources volumes are an aggregates of pressure point sources, and fit the entire data within some regularity conditions (as minimum norm of the anomalous model). The approach works in a step-by-step growth process which allows retrieving very general geometrical configurations (Camacho et al., 2011).

This approach provides interesting results for volcanic areas (Camacho et al., 2011; Samsonov et al., 2014; and Cannavó et al., 2015b), when deformations come from pressure sources. Buoyancy forces of the magma exceed the yield strength of the surrounding rock and, within the ductile lower and mid-crust, diapiric ascent is the main mechanism of magma transport. However, for higher crustal

levels magma transport through fractures is a far more efficient mechanism (Cooper, 1990; Petford et al. 1994). This paper describes a new software developed to implement that published methodology when applied to ground deformations in volcanic areas.

2. Mathematical approach.

The subsurface volume is divided into a 3D partition of (thousands) elemental cells. The aggregation of elemental sources (with superposition of their strain contribution) forms the geometry of the extended pressurized bodies.

The observation equation is [see Camacho et al. (2011) for a detailed description]:

$$ds = ds^{c} + v \qquad (1)$$

where ds, ds^{c} represent, respectively, the vector of observed and calculated three components (3D) of the displacement, and v is the vector for residual values coming from uncertainties in the observation process and the imperfect model fit. The surface deformation, ds^{c}, is calculated as the aggregated effect of different point sources, described by the Mogi model (Mogi, 1958).

The adjustment of the causative structure (inversion problem) is an undetermined problem (especially when inverting data from GPS networks), and some additional constraints are needed to achieve specific solutions. Within a general approach (Tarantola, 1987; Menke, 2012), we solve the inverse problem by means of a mixed minimization condition for residuals v and model magnitude m:

$$v^{T} Q_{D}^{-1} v + \lambda\, m^{T} Q_{M}^{-1} m = \min. \qquad (2)$$

where model vector m is constituted by the pressure values p_{k}, $k=1,...,m$, for the m cells of the model, Q_{D} is the covariance matrix of data, Q_{M} is a suitable covariance matrix corresponding to the physical

3

configuration and λ is a smoothing or regularization factor that balances the goodness of fit and smoothness of the model (Tarantola, 1987). The final solution will be influenced by the assumed smoothing level. Low λ values produce very good data fit but often result in extended and/or irregular models. Conversely, high λ values can produce concentrated and smooth models but with a poorer data fit.

For a simplified treatment, in the attached software, $\boldsymbol{Q}_D^{-1}$ is considered as a diagonal matrix of estimated weights (inverse of data variances) corresponding to the deformation data. $\boldsymbol{Q_M}$ is a suitable covariance matrix corresponding to the physical configuration of cells and data points. This matrix provides a balanced model, avoiding very shallow solutions (see Camacho et al., 2011). The inversion approach is a non-linear problem.

The final source is determined as a free aggregation of a large number of small pressurized sources. The inversion algorithm carries out a step-by-step process of growth of the 3D models, using an exploratory technique to sequentially find the new cell/point source to be set as (de)pressurized and aggregated to the model to improving data fitting (Camacho et al., 2011).

In fact, at the k-th step of the growth process, k cells are filled with the prescribed anomalous values for pressure, obtaining the modelled values $\boldsymbol{ds^c}$. Successively, at the new $(k+1)$-th step, the algorithm searches for a new cell to fill in order to improve the fit following the system:

$$\mathbf{ds} = f \, \mathbf{ds}^c + \mathbf{v} \tag{3}$$

$$misfit = \mathbf{v}^T \mathbf{Q}_D^{-1} \mathbf{v} + \lambda \, f^2 \mathbf{m}^T \, \mathbf{Q}_M^{-1} \mathbf{m} , \tag{4}$$

where $f>1$ is a scale factor, estimated during the inversion, to allow for a fit between the anomaly of the provisional model and the observed anomaly.

90   This inversion methodology has been tested by means of several synthetic tests (Camacho et al,

91   2011), and also by real applications to volcanic environments: Campi Flegrei (Italy) (Camacho et al,

92   2011; Samsonov et al., 2014) and Mount Etna (Italy) (Cannavo et al, 2015b).

93   In the next section, we describe the proposed software tool (PAF-package) that enables a simple

94   and nearly automatic application of this methodology. Then, we present two real applications that

95   illustrate the selection of parameters and some features of the adjusted model for over pressure bodies.

96   Most of the following figures are created by the PAF software.

97   **3. The PAF Software.**

98   The code is in Fortran language and the executable compiled files are obtained with Microsoft

99   Visual Studio Community 2015 for Windows 10 64-bit operating system. The software package

100   consists of two executable files: **ConfigPAF.exe** and **InverPAF.exe** **(Figure 1)**. The first one

101   determines a 3D partition of the subsurface volume into a grid of small parallelepiped cells through

102   a graphical interface for the input of the inversion parameters. It creates an intermediate file

103   (**CellsConfig.txt**) with the information of cell partitions. The second one, **InverPAF.exe**, reads the

104   displacement data and the intermediate file (**CellsConfig.txt**), and runs the inversion to estimate the

105   3D distribution of pressure points that best fit the observed data.
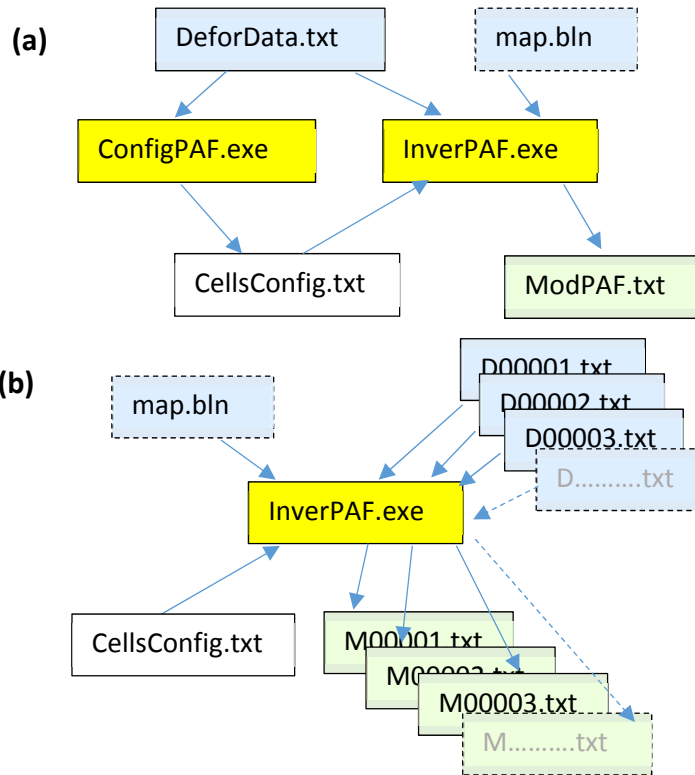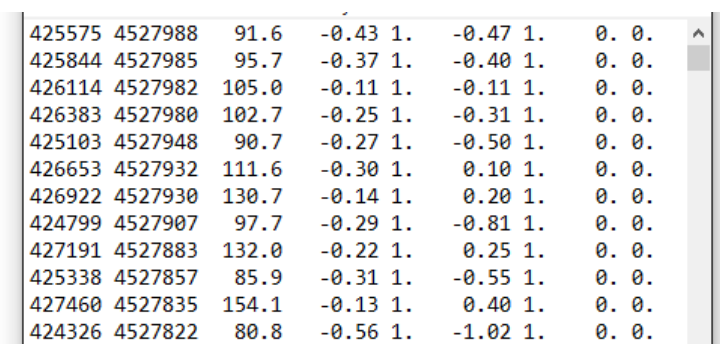
106

107

5

(a)

DeforData.txt — map.bln

ConfigPAF.exe — InverPAF.exe

CellsConfig.txt — ModPAF.txt

(b)

map.bln

D00001.txt
D00002.txt
D00003.txt
D..........txt

InverPAF.exe

CellsConfig.txt

M00001.txt
M00002.txt
M00003.txt
M..........txt

Figure 1. *Scheme of the application of the PAF software. (**a**) Case of deformation data for one observation time (for instance, thousands of pixel data from for a SAR interferogram). (**b**) Sequential application of the inverse approach for successive data files (in blue) producing successive model files (in green) and graphic pictures (case of a monitoring network)*

The PAF software can work in two different ways: (1) statically, considering large displacement data files describing the deformation field (for instance, thousands of pixels with displacement values from SAR interferometry, or combined with GPS data) for a defined time period; and (2) dynamically, through a sequential inversion of successive stages of a deformation process (for instance, successive GPS displacement data obtained at different observation times from a permanent monitoring network).

4. Usage of the software.

4.1. Input files and data.

The 3D deformation data from the several sites are collected in the file **DeforData.txt** (**Figure 2**). This file contains, for each data point, coordinates UTM East-North (m), altitude (m), and deformation values dz (cm, positive upward), dx (cm, positive eastward) and dy (cm, positive northward). The value in the adjacent column, associated to each measurement, indicates a relative weighting value close to 1.0 (smaller values indicate lower quality, higher values indicate higher quality, and zero values indicate observation values not included in the inversion process). This data file can optionally be terminated with an end-of-file character or with a line of zeros.

```
425575 4527988   91.6   -0.43 1.   -0.47 1.   0. 0.
425844 4527985   95.7   -0.37 1.   -0.40 1.   0. 0.
426114 4527982  105.0   -0.11 1.   -0.11 1.   0. 0.
426383 4527980  102.7   -0.25 1.   -0.31 1.   0. 0.
425103 4527948   90.7   -0.27 1.   -0.50 1.   0. 0.
426653 4527932  111.6   -0.30 1.    0.10 1.   0. 0.
426922 4527930  130.7   -0.14 1.    0.20 1.   0. 0.
424799 4527907   97.7   -0.29 1.   -0.81 1.   0. 0.
427191 4527883  132.0   -0.22 1.    0.25 1.   0. 0.
425338 4527857   85.9   -0.31 1.   -0.55 1.   0. 0.
427460 4527835  154.1   -0.13 1.    0.40 1.   0. 0.
424326 4527822   80.8   -0.56 1.   -1.02 1.   0. 0.
```

Figure 2. Input data file DeforData.txt containing coordinates UTM (m), altitude (m), and deformation values dz (cm), dx (cm) and dy (cm) for the data points. Values of 0 and 1 are used to indicate whether the values are included or not, respectively.

A secondary data file is **map.bln**, which can be optionally used to draw the cartography of the studied area. It includes numerical values of polygonal lines (described by the coordinates of the vertexes) with topographical details (roads, etc.).

In the case of sequential application, the data are provided in successive files, named **D*n*.txt**, where *n* is a successive integer number, and with the same format as **DeforData.txt**.

7

4.2. Operational sequence.

Once the data files are set up, the first step to perform an inversion with PAF is to generate a suitable 3D partition of the subsurface volume into a grid of small parallelepiped cells. This step is carried out by using the **ConfigPAF.exe** tool. This program reads the data in **DeforData.txt** (**Figure 2**) and sets several parameters by means of a dialog window (**Figure 3**), offering default values.
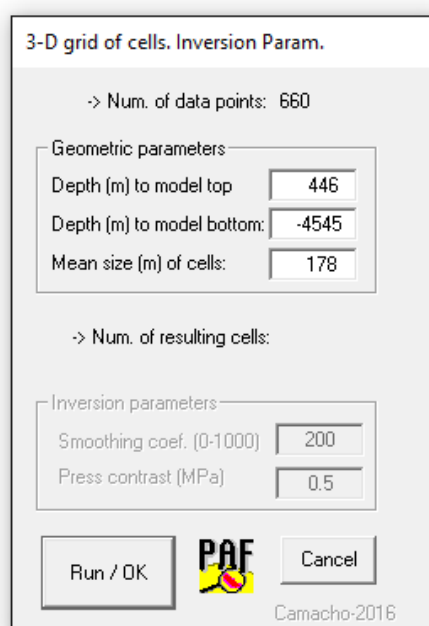
Figure 3. *Input dialog window for the parameters of the 3D grid of cells to prepare the inversion*

calculus.

In the upper part of the Graphical User Interface (GUI) (**Figure 3**), the user can revise the default values for the geometrical parameters of the partition: depth (m above sea level) of the top of the partition volume, depth (m, above sea level) of the bottom of the partition volume, and mean side size (m) of the cells. Once these values are set (pressing Run/OK), the program calculates the resulting number of cells.

Then, in the bottom part of the GUI (**Figure 3**), the program requires two more parameters: (a) the dimensionless smoothing coefficient λ (ranging between 0 and 1000), and, (b) a value for the

8

(positive or negative) pressure contrast throughout the entire anomalous model, ΔP (MPa). The λ coefficient regulates the balance between data fit level and model complexity in the inversion approach. For a low λ value (close to 0), the resulting model becomes very simple, regular and compact, but the data fit can be weak. Conversely, for a high λ value (close to 1000), the data fit is very good (even by fitting some noise component), but the resulting model can be very complex, sometimes even with artefacts. We have imagined some objective criteria (see for instance, Camacho et al. 2007, in other contexts), but for practical applications, we suggest trying different values in a trial and error manner, and to select the most appropriate one considering the resulting models. Some criteria for choosing this value are: be sure that the program finishes the inversion (for too high or too low values of the parameter, the fit conditions are invalid and the program stops); auto-correlated components or significant signal in the residuals should be avoided; the resulting model should be regular and simple (avoiding very small and sparse shallow bodies for noise inversion). For more details, see the two application examples below.

The pressure contrast value ΔP can be selected via trial and error method, by means of doing some iterative runs of the software. For very high values, the model becomes very condensed and compact, and some geometrical details can be lost. Conversely, for very low values the source model becomes larger, with rounding inflated shape. In general, big displacements require strong pressure contrasts and small ones require low-pressure contrasts. We suggest, again, some iterations, trying different values, and observing the resulting anomalous geometry. Nevertheless, the assumed value for ΔP is not a critical value. It mostly concerns the aesthetic aspects of the model. See also application examples below.

Once the **ConfigPAF.exe** is completed (by pressing Run/OK), it creates a new file, namely **CellsConfig.txt**. This is an intermediate file containing (see **Figure 4**): (a) the assumed values for the inversion parameters (smoothing coefficient, pressure contrast, etc.), and (b) the geometrical parameters (location and sides) of the parallelepiped cells.

```
            PAF-modeling of pressure sources

      Parameters
    ------------------------------------------
      5.0    ....Pressure change (MPa)
       30    ....Smoothing coeff. (0<smo<1000)
        5    ....Significance limit  (0<sig<10)
        1    ....Graphic output  0:no  1:YES
        1    ....Number of data epochs
        0    ....First epoch identification
    ------------------------------------------


    Cells: location (UTM, m) and sides (m)
         X      Y      Z     sx   sy   sz
    ------------------------------------------
    428990 4524444    146    196  104  196
    428990 4524544    146    196   94  196
    428990 4524646    146    196  109  196
    428990 4524760    146    196  118  196
    429187 4524437    146    196   89  196
    429187 4524527    146    196   89  196
    429187 4524614    146    196   84  196
    429187 4524699    146    196   84  196
```

***Figure 4**. Intermediate file CellsConfig.txt containing the assumed values for the inversion parameters, and the geometrical parameters (location and sides) of the parallelepiped cells.*

The values of the parameters contained in this file can be manually modified according to the modeller's needs. For instance, the third parameter, "*Significance limit (0<sig<10)*", gives the desired threshold between the significant cells (those close and covered by the data points) from the non-significant cells (those far from the data points). Its default value is 5, but the user can set a different value (for instance, for a low significance threshold, nearly all cells will be considered as significant). The fourth parameter ("*Graphic output 0:no 1:YES*") is used to switch the graphical output during the inversion approach (see below the content of this graphical output). The fifth parameter indicates that the data correspond to only one observation time, or conversely that the inversion has to be carried out in a sequential process of a number (unlimited) of observation times, starting at the first observation time and with the data file identified by the sixth parameter.

Once the file **CellsConfig.txt** is created (and edited), the inversion run by **InverPAF.exe** can start (**Figure 1**). It runs automatically, without any other requirement, and produces an optional

10

194 visualization (fourth parameter in CellCnfig.txt) of the inversion process and of the results on the

195 screen. In the case of sequential application (**Figure 1b**), the **InverPAF.exe** process works

196 continuously, time by time, until it inverts the data of the last observation time. As the final product,

197 the inversion approach creates an output file named **ModPAF.txt** containing the geometrical

198 description of the resulting model, several other parameters of this model, and detailed information

199 about modelled and residual values. These are described further on.

200

4.3. Output files and pictures.

Figure 5 shows an example of the graphical output that can be optionally displayed throughout the inversion approach (see Figure 4 and corresponding description text). This visual information contains graphics about the model growth process and the final results. Statistics about the model growth process are: *misfit* value (see equation 4) evolution, pressure value evolution, planar and vertical cut views (EW and NS) of the aggregation process (significant cells in red and dark blue, no significant cells in yellow and light blue, cells of a previous observation time in green), observed and modelled deformation (along EW and along NS), inversion parameters [step number, pressure value, root mean square (rms) of the residuals, cell depth]. Statistics about the final results are: *misfit* value (equation 4), number of rejected data, number of filled cells, and number of significant cells.
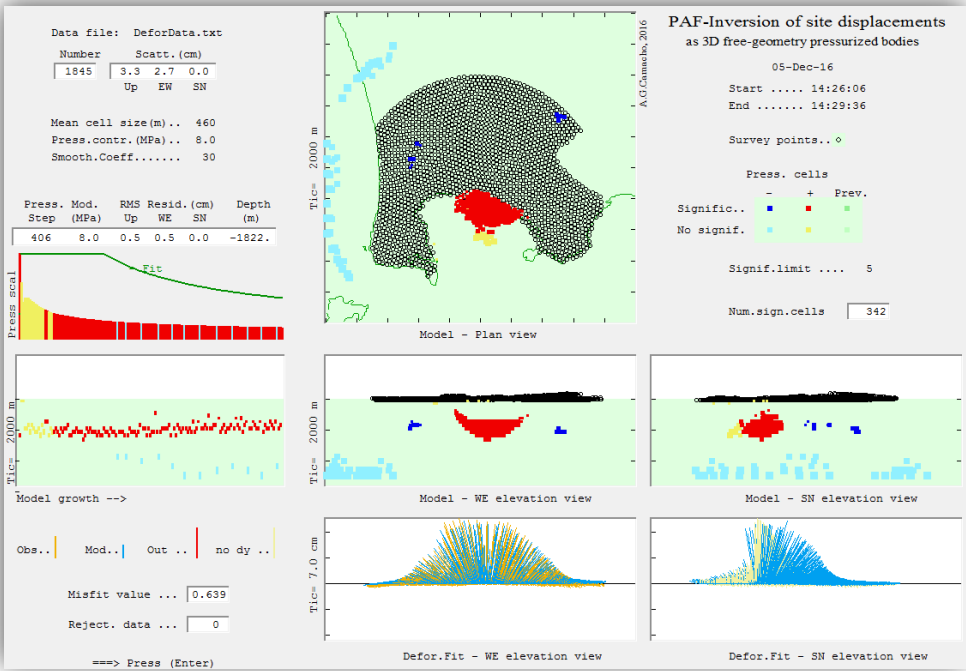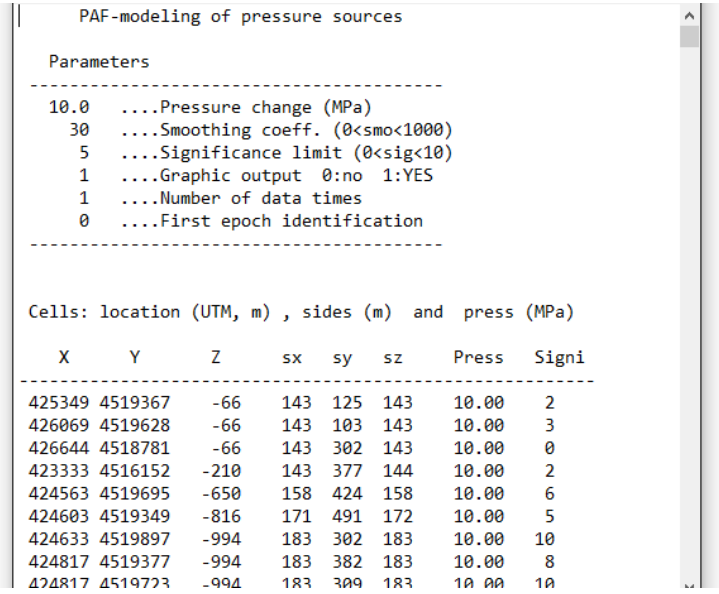
Figure 5. Example of the (optional) screen drawing during the inversion approach. It shows the evolution of the model growth process and various results.

The main product of the PAF inversion is the file **ModPAF.txt**. This file contains the following information:

(1) A copy of the inversion parameters (Figure 6) similar to that in file **CellConfig.txt**.

(2) A list of the pressurized cells (those with no-null pressure values) (see Figure 6). For each cell, the list provides: the UTM coordinates X and Y (m), and the depth Z (m, above sea level) of its geometric centre, the sizes of its sides s_x ,s_y ,s_z (m), the corresponding positive or negative pressure contrast value, and a value for the significance (given by the inverse of the root mean square distance of the cell with respect to the data points, normalized to range from 0 to 20). Higher values of significance correspond to more sensitive cells (this is a measure of how close a given cell is to the data points). This part can be used for further, more sophisticated, drawings of the resulting model.

```
    PAF-modeling of pressure sources

   Parameters
   ----------------------------------------
    10.0   ....Pressure change (MPa)
      30   ....Smoothing coeff. (0<smo<1000)
       5   ....Significance limit (0<sig<10)
       1   ....Graphic output  0:no  1:YES
       1   ....Number of data times
       0   ....First epoch identification
   ----------------------------------------


   Cells: location (UTM, m) , sides (m)  and  press (MPa)

     X      Y      Z     sx   sy   sz    Press  Signi
   --------------------------------------------------
   425349 4519367  -66   143  125  143   10.00    2
   426069 4519628  -66   143  103  143   10.00    3
   426644 4518781  -66   143  302  143   10.00    0
   423333 4516152 -210   143  377  144   10.00    2
   424563 4519695 -650   158  424  158   10.00    6
   424603 4519349 -816   171  491  172   10.00    5
   424633 4519897 -994   183  302  183   10.00   10
   424817 4519377 -994   183  382  183   10.00    8
   424817 4519723 -994   183  309  183   10.00   10
```

Figure 6. *Upper content of the output file **ModPAF.txt**. First, the parameters you use for the run are shown. Then, the list of the filled cells (coordinates, sides, significance) are included.*

13

227   (3) After that, some additional parameters and results about the inversion process are given,

228   followed by a list of the observed, modelled and residual values for the data points (see Figure 7). For

229   each point, the file contains UTM coordinates (m), altitude (m), observed, modelled and residual

230   values (cm) for each component (*dz*, *dx*, *dy*), and an additional value for relative quality weighting

231   (mean value 1) according to the resulting residual values for the three components. This part of the

232   output file can be used for further drawings and statistical analysis of the inversion residuals (see

233   examples below).

234   In the case of sequential application of the PAF inversion approach, for each successive data file

235   **D…....txt** (e.g. **D00016.txt**) corresponding to successive monitoring times (respective sixteenth

236   time), the program generates a model file **M….….txt** (e.g. **M00016.txt**) with the same content as

237   **ModPAF.txt**.

238

239   ***Figure 7.*** *Last part content of the output file ModPAF.txt. Top: End of the list of the filled cells*

240   *(coordinates, sides, significance). Middle: Some parameters and results about the inversion*

241   *process. Bottom: List of the observed, modeled and residual values (cm) for each data point.*

14

In the present version, the maximum number of data points is 10,000 and the maximum number of cells is 100,000, but they can easily be changed in the code.

**5. Case study one: Campi Flegrei inflation.**

Campi Flegrei, one of the most hazardous volcanic areas in the world because of its close proximity to the city of Naples, has been the subject of many studies and surveys (for instance, DeNatale et al., 2006; Manconi et al., 2010; Amoruso et al., 2015; D'Auria et al., 2015; Silvestri et al., 2015; Trasatti et al., 2015; Bagagli et al., 2017). Samsonov et al. (2014) applied the multidimensional small baseline subset (MSBAS) differential interferometric synthetic aperture radar (DInSAR) technique to obtain vertical (Up) and horizontal components (EW) of ground deformation for Campi Flegrei spanning 20 years. They used radar images from ERS, Envisat (European Space Agency), and RADARSAT-2(Canadian Space Agency) satellites. Their results show that the area underwent continuous subsidence from 1993 through 1999, followed by several alternate periods, and a moderate uplift which began in 2007 and increased through 2012, reaching about 17 cm by 2013. We study the uplift period from 2007/10/03 to 2013/06/15, taking as input data the accumulated 2D deformation (Up and EW components). Some characteristics of this case for applying of the software are: (1) large number of data points (SAR pixels), (2) lack of NS component in the data, (3) data from one isolated observation time, (4) strong deformation, and, consequently, (5) high signal/noise ratio in the data.

From the thousands of pixels obtained by Samsonov et al. (2014), we have selected 1845 pixels covering the anomalous area and allowing for a fast execution. The sub-sample methodology selects those points with two arbitrary conditions: (1) mutual distance larger than 250 m, and (2) distance to the centre of deformation smaller than 8 km. Figure 8 shows the distribution of the selected pixels and the feature of the vertical component (with more than 12 cm accumulated in the central area).

265   Once the 3D deformation data for the 1845 pixels is arranged in the file **DeforData.txt**, we can

266   apply the described process and software. The program **ConfigPAF.exe** suggests as default values:

267   437 m for altitude of the model top, -5915 m for depth of the model bottom, and 231 m for mean cell

268   side. We accept the first two values, but we try 180 m for mean cell side, looking for a higher

269   resolution of the deformation source. For this new value, the resulting number of cells is 72017, as

270   provided by the program.

271   Then, the program suggests the default values: 200 for smoothing coefficient, and 0.5 MPa for

272   pressure contrast. They are very general values. We choose more suitable values for these parameters

273   by means of trial and error, looking for suitable morphology of the resulting model. For this particular

274   case of Campi Flegrei, we have a very strong accumulated deformation field, and it requires a higher

275   pressure contrast. After some trials, we select 10.0 MPa (accumulated pressure for the anomalous

276   volume elements) as a tentative model contrast (the anomalous structure becomes very inflated for

277   smaller values).

278

279

280
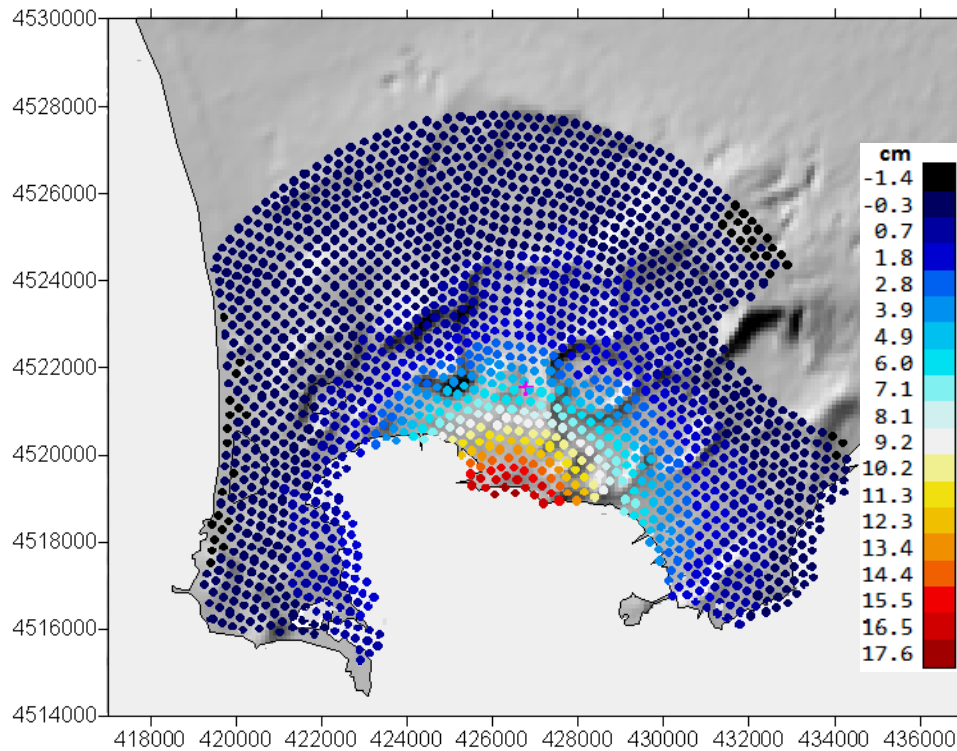
Figure 8. *Selected pixels and vertical deformation (cm) (annual linear rate) for the inflation episode in Campi Flegrei (Italy). UTM coordinates. Uplift period 10/2007-06/2013.*

Regarding the smoothing coefficient λ, the general value 200 can be appropriate for the more common cases. In this case of strong deformation, the signal/noise ratio is very high (see below, final residual level with respect to data scattering level), and the model does not require a high smoothing value. After some trials, we selected 10 as the suitable smoothing value. Nevertheless, the difference between models obtained with different inversion values is not critical (by way of example, Figure 5 shows the model obtained with a value of 30 for smoothing and 8.0 MPa for accumulated pressure).

Once these values are selected, the rest of the inversion approach is nearly automatic. The number of observation times is one in this case. We accept the general value 5 for the significance limit. Figure 9 shows the resulting model by means of planar and vertical cut views. The model consists

mostly of an anomalous body, at a mean depth about 1.8 km, composed of overpressure cells (red colour for significant cells and yellow for non-significant cells). The morphology of the anomalous structure as a "partially filled parabolic glass" suggests a shallow (depth 1-2 km) hydrothermal system confined to the caldera fill materials. This result is very similar in geometry to that obtained in Camacho et al. (2011) for the uplift period 1992-2000.

The final residual values after the inversion approach (root mean square values of 0.5 cm for Up, and EW components) are fairly small with respect to the total scattering of the deformation data (3.3 cm and 2.7 cm accumulated for Up and EW, respectively), confirming the suspected good ratio signal/noise in the present deformation case.

Figure 9 also shows two vertical views of the fit between observed (orange lines) and modelled (blue lines) deformations in the bottom. Light yellow lines correspond to dz data without dy values, the approach determines modelled values also for dy. In this figure, we can also observe the presence of several areas with non-significant cells (light blue and yellow ones), mostly in peripheral areas. These artificial structures are introduced by the inverse approach to absorb distortion effects contained in the interferometric data. Such fictitious bodies allow the significant structures to be nearly free of distortion components in the data.
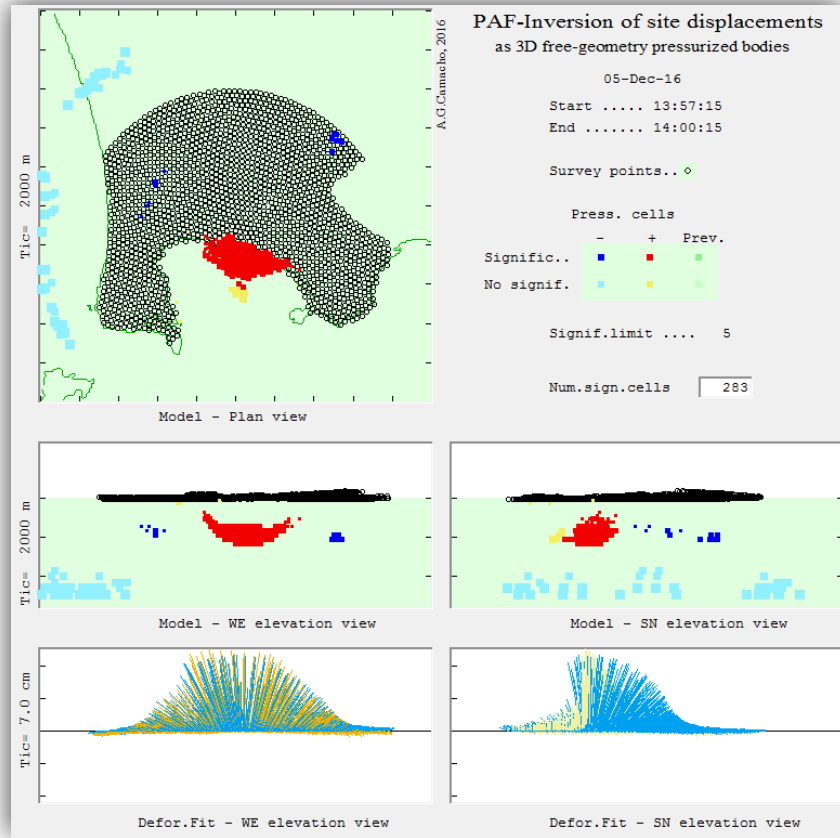
308

Figure 9. *Resisting inversion model for the Campi Flegrei inflation data* <mark>*showing the source*</mark> *as a subsurface anomalous structure (about 1.8 km mean depth) of aggregated overpressure cells.*

<mark>6. Case study two: Etna monitoring.</mark>

A second example regards the sequential application of the PAF software to a network of 31 permanent GPS stations close to Mt. Etna (Sicily, Italy) (Cannavò et al., 2015b and references on it), see Figure 10. Mt. Etna, situated on the eastern coast of Sicily, is a large basaltic volcano built up in a geodynamic setting generated during the Neogene convergence between the African and European plates (Allard et al., 2006; Branca et al., 2011) and is one of the most active volcanoes in the world. Its activity comprises strombolian activity, which may evolve into lava fountains and effusive events, and lateral eruptions occurring along fractures (Aloisi et al., 2006; Cannavò et al., 2015a).
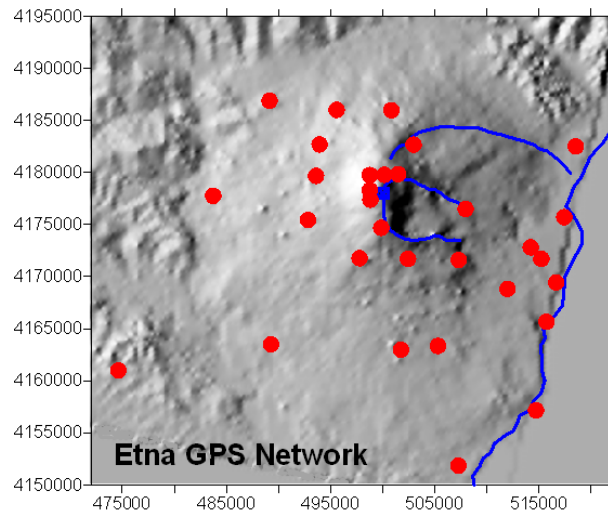
Figure 10. *Location of a network of 31 permanent GPS stations close to Mount Etna volcano (Sicily, Italy). UTM coordinates are indicated.*

We analyse the three component (Up, EW, NS) deformation data corresponding to 8 successive fortnightly periods, from May/2007 to September/2007 (Cannavò et al., 2015b). The data are arranged into sequential files, one for each period or observation time, containing the deformation at the network stations for each period. Some characteristics of this application of the software are: (1) small number of data points (GPS stations), (2) information on the three components of the displacement in the data, (3) sequential application for several observation times, (4) small deformation, and, consequently, (5) low signal/noise ratio in the data.

The PAF software is applied taking into account the peculiarities of the case. The **CellsConfig.exe** program suggests the following values: depth of the model top = 3131 m (above sea level), depth of the model bottom = -15859 m (positive above sea level), and mean side of cells = 658 m. We accept these default suggestions. Then, the resulting number of cells is 33250. Next, the program suggests the usual general values for the smoothing coefficient (200) and for the pressure contrast (0.5MPa).

The suggested pressure value 0.5 MPa is small, and we accept it as suitable for this case (displacements are not very large, and therefore causative anomalous pressure should also not be very large).

However, in this case, for the considered monitoring network the general smoothing value 200 looks too small. In fact, in this case the number of data points is very small (31 stations), the measured displacements are not large, and GPS data set presents a low signal to noise ratio for the considered time periods. We have an estimated inaccuracy level of about 0.1 - 0.3 cm in the fortnightly period, with respect to the deformation level (displacement data scattering) of about 0.3 - 0.6 cm. Therefore, we need to introduce a bigger smoothing coefficient to control the high noise level and avoid fictitious structures. After some trial and error running of the code, we have selected the value 600 as a suitable smoothing.

Then, after these selections, the inversion approach is nearly automatic. We use the usual significance limit 5, and in this case we analyse 8 observation times, starting in the time 10 (so our data files will be **D00010.txt**, **D00011.txt**, …., **D00017.txt**). The program **InverPAF.exe** takes only some seconds to carry out the inversion for each period, and to produce the drawings and the respective output files.

Usually, the displacement results from the monitoring network, for most of the deformation periods without an eruptive episode, do not show a significant deformation. However, we have selected a particular sequence of periods (8 successive periods, from May/2007 to September/2007) that show an apparent intrusive episode; see Cannavò et al. (2015b) and references therein. Figure 11 shows some figures from the program display of the resulting model for the sequential study. We can observe some features. For the initial observation times (e.g. times (a) and (b)), the model does not show significant pressure cells (red, for pressure increase, or dark blue, for pressure decrease). There are many filled cells, but in non-significant locations (yellow or light blue) (low-sensitive cells),

358   which look like artefact sources, and are introduced by the inversion program to model some global

359   noisy pattern.

360   For the next observation times, (c) to (f), we infer a distributed pressure source that ascends in the

361   central zone with a certain inclination towards the east, reaching a minimum depth about 3 km below

362   sea level. This structure is similar to that modelled in Cannavó et al. (2015b). Green cells in the figure

363   indicate cells from the previous observation time, allowing following the evolution of the anomalous

364   structures from one to another observation time.

365   Times (g) and (h) return to the non-significant values of pressure changes. For observation time

366   (h), the program detects and rejects outlier observation data (denoted in red in the corresponding data

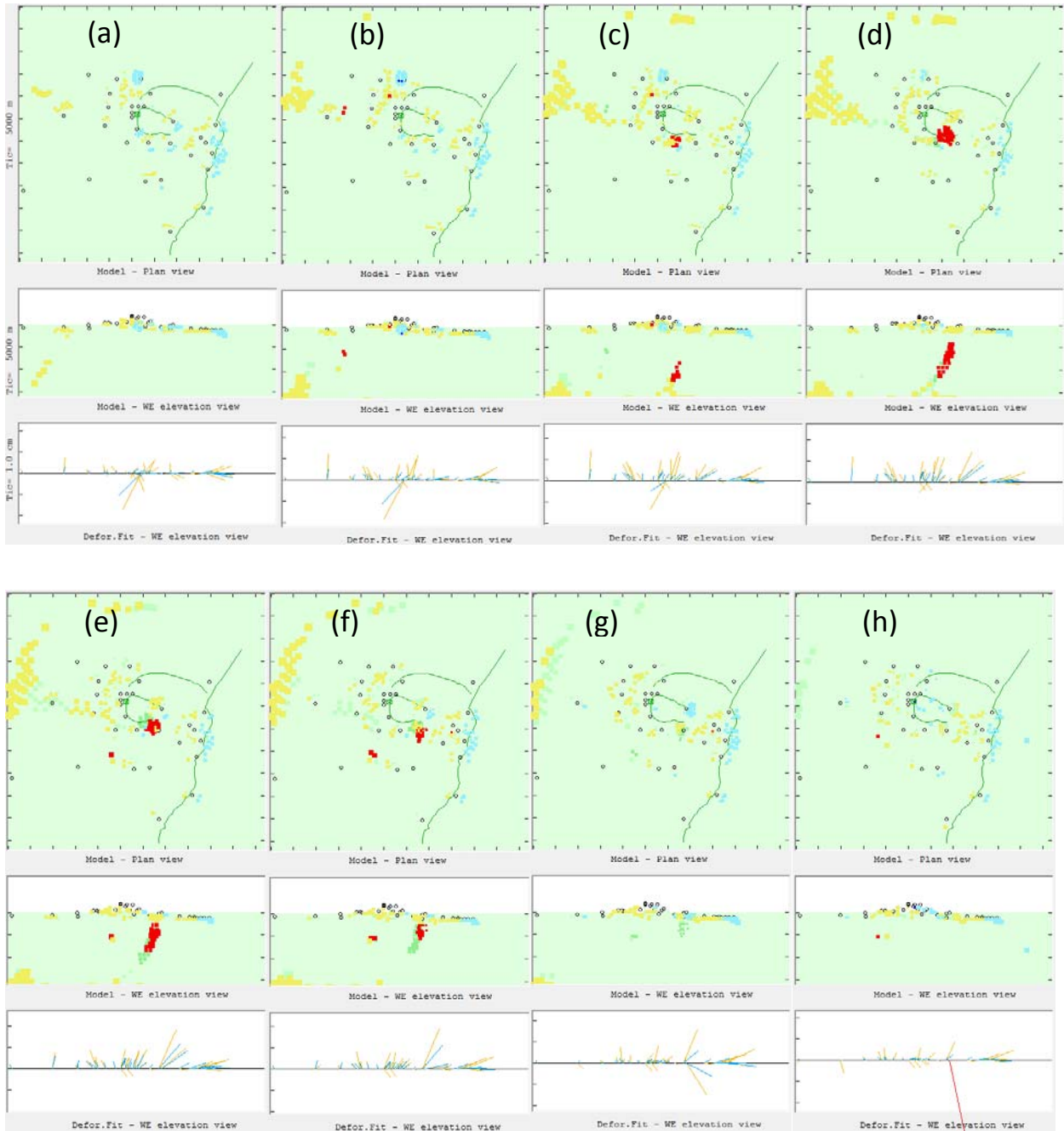367   panel in Figure 11).

368

369

370

Figure 11. Planar and WE elevation views of the successive inversion models obtained in the sequential monitoring for the Etna network (biweekly data, from May to September 2007). Yellow and light blue cells indicate non-significant cells (fictitious structures to absorb data distortions). Observation times (c) to (f), with a significant high pressure body (red colour), suggest an intrusive episode. Tip step in axes corresponds to 5 km.

23

7. Conclusions

PAF software allows carrying out an inversion, in a nearly automatic mode, of displacement data (1D to 3D) obtaining extended 3D sources of overpressure bodies with free geometry. An elastic half-space response is assumed for the deformation calculus for each elementary source. The source bodies are described as aggregations of small cells filled with the prescribed pressure contrast. It works particularly well for volcanic areas, where deformations can be supposed as (mainly) due to subsurface pressure sources.

The software requires tuning by choosing suitable values for two main parameters in the inversion approach: the smoothing coefficient λ (which controls the balance between data fit and model regularity in the regularity conditions) and the basic pressure contrast (in MPa). Suitable values for both parameters are normally selected in a trial and error way, looking for good model features (regularity, size, etc.) and good residual distribution (null autocorrelation of residuals). Nevertheless, the choice of these parameters is not too critical with respect to the main features of the resulting model.

As shown in the application examples, the software can work for large data sets (for instance, coming from InSAR data), and for reduced sets of sequential data (for instance, coming from a small GPS monitoring network). It can work for fully 3D data, or also for 1D or 2D data (using e.g. GNSS, InSAR, or levelling data). For both application examples, geometry of the resulting models offers interesting features to evaluate the deformation causative phenomenon.

This software consists of two executable programs, and can be freely downloaded from the repository PAF-software at github.com or by asking the corresponding author. The first program (**ConfigPAF.exe**) allows the user to set (in a dialog mode) the values for the inversion parameters, and for the geometrical configuration of the small cells. The second program (**InverPAF.exe**) works with the results of the former program, and does not require any user input (display of intermediate

or final result is optional). It can be incorporated into a larger software tool for monitoring at a volcanic observatory and can even run automatically in real time, giving also very useful results (see Cannavò et al., 2015b). The source codes, user manual, executable files and a test example (including input data and results) can be obtained on request from the corresponding author, under an open source license.

References.

Allard, P., Behncke, B., D'Amico, S., Neri, M., and Gambino, S. (2006) Mount Etna 1993–2005: anatomy of an evolving eruptive cycle, Earth-Sci. Rev., 78, 85–114, doi:10.1016/j.earscirev.2006.04.002.

Aloisi, M., Bonaccorso, A., and Gambino, S. (2006) Imaging compositive dike propagation (Etna, 2002 case), J. Geophys. Res., 111, B06404, doi:10.1029/2005JB003908.

Amoruso, A., Crescentini, L., Scarpa, R., Bilham, R., Linde, A. T., and Sacks, I. S., 2015. 511 Abrupt magma chamber contraction and microseismicity at Campi Flegrei, Italy: Cause and 512 effect determined from strainmeters and tiltmeters, J. Geophys. Res. Solid Earth, 120, 513 5467–5478, doi:10.1002/2015JB012085.

421 Bagagli, M., Montagna, C. P., Papale, P., and Longo, A., 2017. Signature of magmatic processes 532

422   in strainmeter records at Campi Flegrei (Italy), Geophys. Res. Lett., 44, 718–725, 533

423   doi:10.1002/2016GL071875.

424 Battaglia, M., and Hill, D.P. (2009), Analytical modeling of gravity changes and crustal deformation

425   at volcanoes: The Long Valley caldera, California, case study, Tectonophysics, 471, 45-57, doi:

426   10.1016/j.tecto.2008.09.040.

427 Battaglia, M., Cervelli, P.F., and Murray, J.R., 2013, Modeling crustal deformation near active faults

428   and volcanic centers—A catalog of deformation models: U.S. Geological Survey Techniques

429   and Methods, book 13, chap. B1, 96 p., http://pubs.usgs.gov/tm/13/b1.

430 Branca, S., Coltelli, M., and Groppelli, G. (2011) Geological evolution of a complex basaltic

431   stratovolcano: Mount Etna, Italy, Ital. J. Geosci., 130, 306–317, 2011. doi: 10.3301/IJG.2011.13.

432 Camacho, A. G., González, P. J., Fernández, J., & Berrino, G. (2011) Simultaneous inversion of

433   surface deformation and gravity changes by means of extended bodies with a free geometry:

434   Application to deforming calderas. J. Geophys. Res., 116, B10401.

435   doi.org/10.1029/2010JB008165

436 Camacho, A. G., J. C. Nunes, E. Ortiz, Z. França, and R. Vieira (2007), Gravimetric determination

437   of an intrusive complex under the Island of Faial (Azores): Some methodological improvements,

438   Geophys. J. Int., 171, 478–494, doi:10.1111/j.1365-246X.2007.03539.x.

439 Cannavó, F., Arena, A., & Monaco, C. (2015a). Local geodetic and seismic energy balance for

440   shallow earthquake prediction. Journal of Seismology, 19(1), 1-8, doi:10.1007/s10950-014-

441   9446-z.

442 Cannavò, F.; Camacho; A.G.; González, P.J.; Mattia, M.; Puglisi, G; and Fernández, J. (2015b) Real

443   Time Tracking of Magmatic Intrusions by means of Ground Deformation Modeling during

444   Volcanic Crises, Scientific Reports, 5:10970. doi: 10.1038/srep10970

445   Charco, M., Fernández, J., Luzón, F., Tiampo, K.F., and Rundle, J.B. (2007), Some insights into

446   topographic, elastic a self-gravitation interaction in modelling ground deformation and gravity

447   changes in active volcanic areas, Pure Appl. Geophys., 164, 865-878, doi 10.1007/s00024-004-

448   0190-y.

449   Cooper, R. F., 1990. Differential stress-induced melt migration, an experimental approach. Journal

450   of Geophysical Research 95, 6979-6992.

451   D'Auria, L., Pepe, S., Castaldo, R., Giudicepietro, F., Macedonio, G., Ricciolino, P., Tizzani, 612 P.,

452   Casu, F., Lanari, R., Manzo, M., Martini, M., Sansosti, E., and Zinno, I., 2015. Magma 613

453   injection beneath the urban area of Naples: a new mechanism for the 2012–2013 volcanic 614

454   unrest at Campi Flegrei caldera, Scientific Reports 5, 13100, doi: 10.1038/srep13100.

455   De Natale, G., C. Troise, F. Pingue, G. Mastrolorenzo, L. Pappalardo, and E. Boschi (2006), The

456   Campi Flegrei caldera: Unrest mechanisms and hazards, in Mechanisms of Activity and Unrest

457   at Large Calderas, edited by C. Troise, G. De Natale, and C. R. J. Kilburn, Geol. Soc. London

458   Spec. Publ., 269, 25–45.

459   Dzurisin D. (2003), A comprehensive approach to monitoring volcano deformation as a window on

460   the eruption cycle, Rev. Geophys., 41(1), 1001, doi:10.1029/2001RG000107.

461   Lisowski, M. (2007), Analytical volcano deformation source models, in Volcano Deformation, chap.

462   8, pp. 279-304, Springer Praxis, Chichester, U.K.

463   Manconi, A., Walter, T. R., Manzo, M., Zeni, G., Tizzani, P., Sansosti, E., and Lanari, R., 2010. 766

464   On the effects of 3-D mechanical heterogeneities at Campi Flegrei caldera, southern Italy, 767

465   J. Geophys. Res., 115, B08405, doi:10.1029/2009JB007099.

466   Masterlark, T. (2007), Magma intrusion and deformation predictions: Sensitivities to the Mogi

467   assumptions, J. Geophys. Res., 112, B06419, doi:10.1029/2006JB004860.

468   Menke, W. (2012) Geophysical Data Analysis: Discrete Inverse Theory. Academic Press/Elsevier,

469   330 p. ISBN: 978-0-12-397160-9.

Mogi, K. (1958), Relations between the eruption of various volcanoes and the deformation of the ground surface around them. Bull. Earthquake Res. Inst. Univ. Tokyo, 36, 99-134.

Pedersen, R., Sigmundsson, F., 2006. Temporal development of the 1999 intrusive episode in the Eyjafjallajokull volcano, Iceland, derived from InSAR images. ¨ Bull. Volcanol. 68, 377–393.

Petford, N., Lister, J. R., Kerr, R. C., 1994. The ascent of felsic magmas in dykes. Lithos 32, 161-168.

Rymer, H and Williams-Jones, G. (2000). Volcanic eruption prediction: Magma chamber physics from gravity and deformation measurements. Geophys. Res. Lett., 27-16, 2389-2392. doi: 10.1029/1999GL011293.

Saltogianni, V., S. C. Stiros, A. V. Newman, K. Flanagan, and F. Moschas (2014), Time-space modeling of the dynamics of Santorini volcano (Greece) during the 2011–2012 unrest, J. Geophys. Res. Solid Earth, 119, doi:10.1002/2014JB011409.

Samsonov, S. V., Tiampo, K. F., Camacho, A. G., Fernández, J., and González, P. J. (2014) Spatiotemporal analysis and interpretation of 1993–2013 ground deformation at Campi Flegrei, Italy, observed by advanced DInSAR. Geophys. Res. Lett., 41, 6101–6108 (2014). doi:10.1002/ 2014GL060595.

Tarantola, A. (1987), Inverse Problem Theory, Elsevier, Amsterdam, 613 pp.

Trasatti E., Polcari M., Bonafede M., Stramondo S. (2015). Geodetic constraints to the source mechanism of the 2011-2013 unrest at Campi Flegrei (Italy) caldera. Geophysical Research Letters, 10.1002/2015GL063621.

Silvestri M., Diaz J.A., Marotta E., Musacchio M., Buongiorno M.F., Sansivero F., Cardellini C., Pieri D., Amici S., Bagnato E., Beddini G., Belviso P., Carandente A., Colini L., Doumaz F., Peluso R., Spinetti C. (2015). Use of multiple in situ and remote sensing instruments and techniques at Solfatara field campaign for measurements of CO2, H2S and SO2 emissions: special demonstration on unmanned aerial systems. Quaderni di Geofisica, n. 129, Anno 2015

495   Willians, C.A., and Wadge, G. (1998), The effects of topography on magma chamber deformation

496   models: Application to Mt. Etna and radar interferometry, Geophys. Res. Lett., 25, 1549-1552.